Aortic root sizing for transcatheter aortic valve implantation using a shape model parameterisation

Title: Aortic root sizing for transcatheter aortic valve implantation using a shape model parameterization

Authors:

Bart Bosmans[1,2,3], Toon Huysmans[4], Patricia Lopes[1,2,4], Eva Verhoelst[2], Peter Mortier[5], Peter de Jaegere, Jan Sijbers[4], Jos Vander Sloten[1], Johan Bosmans[3]

Affiliations:

[1] KULeuven, Faculty of Engineering Science, Celestijnenlaan 300C, 3001 Leuven, Belgium. Department of Mechanical Engineering, Biomechanics Section

[2] Materialise N.V., Technologielaan 15, 3001 Leuven, Belgium

[3] University of Antwerp, Faculty of Medicine and Health Sciences, Universiteitsplein 1, 2610 Antwerp, Belgium. Department of Translational Pathophysiological Research, Cardiovascular diseases

[4] University of Antwerp, imec-Vision Lab, Universiteitsplein 1, 2610 Antwerp, Belgium.

[5] FEops N.V., Technologiepark-Zwijnaarde 603 Ghent, Belgium

Corresponding author:

Bart Bosmans

KULeuven – Departement of Mechanical Engineering, Biomechanics Section

Technologielaan 15,

3001, Leuven, Belgium.

Tel: +32 16 396 728

Fax: +32 16 396 606

Bart.Bosmans@kuleuven.be

Abstract:

During a transcatheter aortic valve implantation, an axisymmetric implant is placed in an irregularly shaped aortic root. Implanting an incorrect size can cause complications such as leakage of blood alongside or through the implant. The aim of this study was to construct a method that determines the optimal size of the implant based on the 3-dimensional shape of the aortic root. Based on the pre-interventional computed tomography scan of 89 patients, a statistical shape model (SSM) of their aortic root was constructed. The weights associated with the principal components of the SSM served as a parametric description of each aortic root. These weights and the volume of calcification in the aortic valve were used as parameters in a generalized linear model and a random forest classifier. Both classification algorithms were trained using the patients with no or mild leakage after their intervention. Subsequently, the algorithms were applied to the patients with moderate to severe leakage. The random forest classifier was accurate in 96% of the training cases. 55% of the patients with moderate to severe leakage were assigned a different size implant, 11 out of those 20 got one size smaller. The proposed method was capable of accurately and semi-automatically determining an implant size, using a CT scan of the aortic root. Further research is required to assess whether the different size implants would improve the outcome of those patients.

Introduction

Aortic valve stenosis is the most commonly acquired valvular heart disease in the elderly. Despite advances in cardiac surgery and low mortality rates after conventional surgical aortic valve replacement, up to one third of patients with symptomatic aortic valve stenosis are not considered for valve replacement, often due to age, frailty or co-morbidities [Bose et al., 2007; Thourani et al., 2011]. Transcatheter aortic valve implantation (TAVI) has been proven to be a reasonable alternative for the treatment of aortic valve stenosis in elderly (very) high-risk patients [Kodali et al., 2012].

During the TAVI procedure an axisymmetric device is implanted in the patient´s aortic root. In case of the CoreValve devices (Medtronic Inc., Minneapolis, MN, USA), four sizes are available, they have a 23 mm, 26 mm, 29 mm or 31 mm bottom cross-sectional diameter respectively. The CoreValve size range is used to treat patients with an annulus diameter between 18 mm and 29 mm [Holmes et al., 2012]. The current planning procedure uses computed tomography (CT) images to size the annulus, the ring formed by the bottom of each valve leaflet. The annulus diameter can be calculated based on the perimeter, the cross-sectional surface area or the minimum and maximum diameter [Buzzatti et al., 2013; Hayashida et al., 2012]. However, the aortic root and the implants are 3-dimensional structures, the aortic root is rarely cylindrical and a suboptimal implant size can lead to complications such as aortic regurgitation [AR] [Détaint et al., 2009; Jilaihawi et al., 2012].

Determining the size of the implant based on the 3-dimensional (3D) shape of the aortic root might reduce complication and the observer dependency. Therefore, the goal of this research is to construct a method with which the implant size can be accurately estimated based on a parametric description of the 3D aortic root.

A statistical shape model (SSM) is a common method to generate a parametric description of a population of 3D shapes. In this type of model, each shape is described as a deviation from the average of the population along the principal components of variation. SSMs have multiple applications in characterizing anatomical variability, for example, investigating the difference

between the brain anatomy of healthy people versus schizophrenics [Ferrarini et al., 2008] or Alzheimer patients [Wang et al., 2013]. SSMs are also used to investigate the shape variation in bone structures such as the human ear canal [Paulsen et al., 2002] and to reconstruct missing, malformed or fractured bone structures [Ren et al., 2014; Zachow et al., 2005]. In addition, SSMs are used to model the whole body [Magnenat-thalmann et al., 2004] or a part, such as the scalp [Lacko et al., 2015] to provide a design space for clothing for example.

Materials & method

89 patients received a contrast enhanced ECG-triggered, end diastolic CT scan prior to the TAVI procedure in which a CoreValve was implanted. The scans were performed on a 64-slice GE lightspeed (General Electric Company, Easton Turnpike, Fairfield, CT, USA) with a spatial resolution of 0.6 mm. All patients received an intravenous injection of 80ml of contrast agent at a flow rate of 4 ml/s, followed by 30 ml at 2.5 ml/s. The minimum diameter, the maximum diameter, the diameter based on the perimeter and the diameter based on the surface area of the aortic annulus were taken into account to determine the size of the implant [Schultz et al., 2010]. One patient received a 23 mm implant, 23 patients received a 26 mm implant, 50 patients received a 29 mm implant and 15 received a 31 mm implant. AR was graded immediately after the implantation on the procedural angiography, as described by Seller et al. [Sellers et al., 1964].

Image analysis

Segmentation was performed on the pre-operative scans using Mimics 16.0 (Materialise N.V., Leuven, Belgium) to extract the 3D shape of the aortic root. The left ventricle and aorta were extracted from the CT images using a threshold on the contrast agent in the blood, as depicted in figure 1A. The left ventricle and aorta were separated from connected structures and each other using a graph cut algorithm [Boykov and Kolmogorov, 2004] (figure 1D). 3D triangulated parts of the blood volume and the separate chambers were created using a marching cubes triangulation (figure 1B and E). Smoothing was performed to remove noise and small substructures. The aortic root was

cut from the 3D part to create a tubular model using a plane perpendicular to the centerline at the level of the mitral valve and the aortic arch (figure1C). Three leaflets were created starting from the left ventricle model by smoothing and disconnecting the valve surface (figure 1E). Finally, the calcifications were extracted using a threshold of 800 Hounsfield units, which is a consistently higher intensity compared to the contrast agent in the majority of patients. A region grow was applied to select the calcifications attached to the aortic valve, followed by a marching cubes triangulation to convert the pixels into a 3D model. Finally, the internal volume of the calcifications was computed.

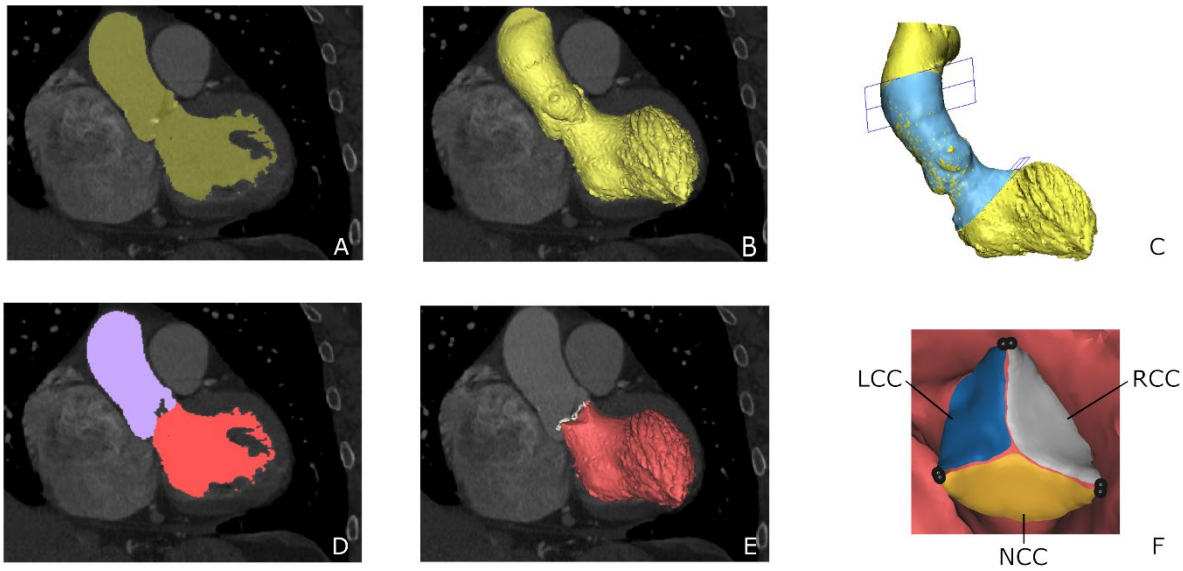

Figure 1: ((A) Coronal view of a computed tomography scan with the left ventricle and aorta blood pool colored yellow. (B) Three dimensional (3D) reconstruction of the geometry. (C) The tubular aortic root model. (D) Split of the blood pool in aorta and left ventricle. (E) The 3D reconstruction of the left ventricle and aortic valve calcifications. (F) The individual leaflets and commissure points used in the shape model generation.

Generate the shape model

The next step was to establish correspondence in the population of surface models. The tubular shape of the aortic root and the leaflets were corresponded using two different methods. The construction of the correspondence for tubular surfaces was described in detail in [Huysmans et al.,

2010]. Briefly, first the tubular part of each aortic root was mapped to an open-ended cylinder. Next, the shapes were aligned using their principal axes, then the alignment of the parameterization was determined by minimizing the description length of the SSM [Davies et al., 2002]. Finally, both the spatial alignment and the parameterization were optimized simultaneously with respect to the minimum description length.

The correspondence in the leaflets was determined using a mapping of each leaflet on a disk with diameter one. The mapping was determined by representing each point on the surface as a linear combination of its neighbors. This resulted in a system of linear equations that has a unique solution, given that the points on the boundary that were positioned on the disk boundary at a relative distance equivalent to the distance along the boundary of the leaflet. The disks were aligned along the section of the boundary between the leaflet commissures which denotes the attachment to the aortic wall. Next, a Laplacian smoothing was performed on the first instance of each of the three leaflets, in order to generate a more uniform mesh for all the leaflets. The smoothing substitutes each point with the average of its neighbors, constructing the master parameterization. Subsequently, the points of this master parameterization were transformed to each patients' leaflets. The transformation is determined by describing the coordinates of the master in function of the triangles of the target leaflet using the disk parameterization of both the target and the master.

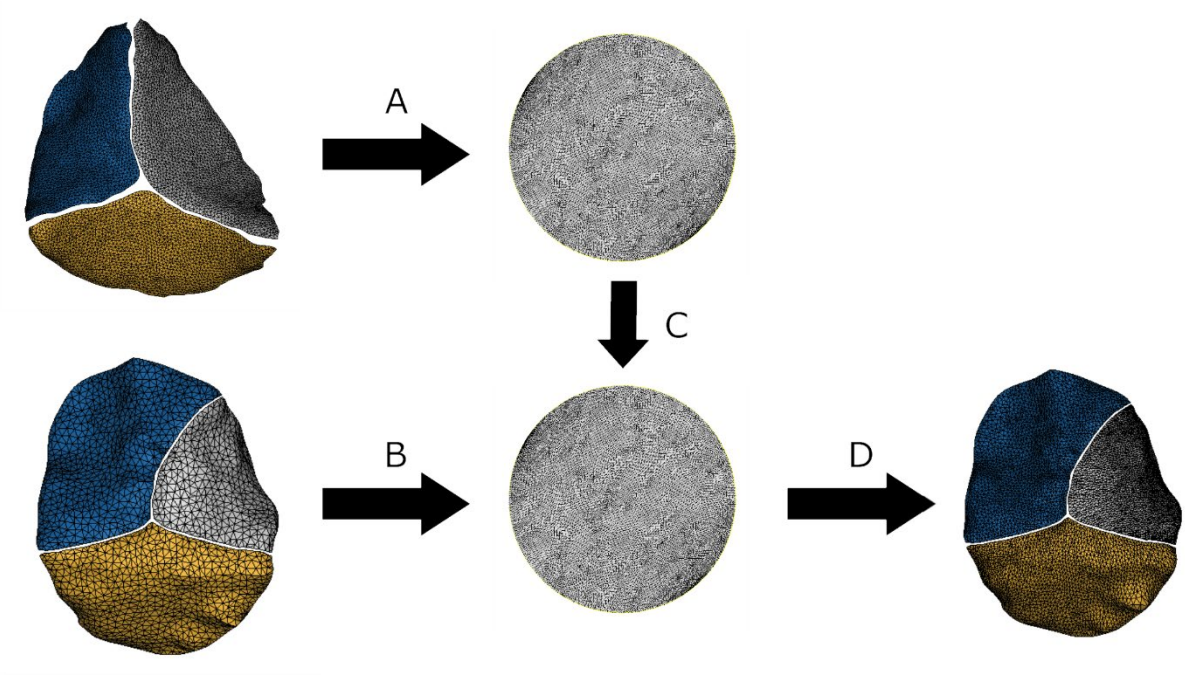

Figure 2: (A) parameterization of the master leaflet on a disk with diameter 1. (B) Parameterization of a sample leaflet on a disk. (C) Registration of the master parameterization on the sample using the commissure points. (D) Transformation of the corresponding points of the master parameterization to the sample leaflet.

Next, the SSM is built, first the spatial registration derived from the aortic root parameterization was applied to the leaflets to position them correctly inside each shape. The shapes are represented as a vector $\boldsymbol{x_i} = \left[x_{i,1}, y_{i,1}, z_{i,1}, \ldots, x_{i,n}, y_{i,n}, z_{i,n}\right]$ and put into a matrix as columns. After subtracting the mean shape $\bar{\boldsymbol{x}}$,

$$\boldsymbol{A} = \left[\boldsymbol{x_1^T} - \bar{\boldsymbol{x}}^{\boldsymbol{T}} \ldots \boldsymbol{x_m^T} - \bar{\boldsymbol{x}}^{\boldsymbol{T}}\right]$$

a principal component was applied. Each aortic root could then be represented as a sum of the mean and the weighted principal components:

$$\boldsymbol{x} = \bar{\boldsymbol{x}} + \boldsymbol{Ub}$$

where $\boldsymbol{x}$ is a new shape, $\boldsymbol{U}$ a matrix with the principal components as columns and $\boldsymbol{b}$ a column vector of the weights of the principal components.

The quality of the SSM was characterized using the compactness, generalization ability and specificity [Huysmans et al., 2010; Styner et al., 2003]. The compactness was calculated as the percentage of the total variance present in the first n principal components:

$$C(n) = \frac{\sum_{i=1}^{n} \lambda_i}{\sum_{i=1}^{m} \lambda_i}$$

where λ_i is the variance of the ith principal component and *m* the total number of principal components. The generalization ability is a measure for the ability of the SSM to approximate a shape which is not in the model and was calculated using a leave-one-out experiment. The specificity measures how close random samples, generated by the model are to the shapes in the population.

Sizing classification

The principal component analysis aggregates the total shape variation in a limited number of independent principal components. Therefore, a good approximation of a shape can be obtained using only a limited number of the principal components. In the aortic root model 95% of all variation was described by the first 20 principal components.

The patients were divided in two subgroups: the first group had AR grade 0 – 1, the second group had an AR grade ≥ 2. The first group was used to train two different classification algorithms, a generalized linear model and a random forest classifier of 10 trees with a maximum depth of 5 branch points [Pedregosa et al., 2011]. The weights of the first 20 principal components and the aortic valve calcification volume were used as parameters to describe each patient. In a first step, these parameters were ranked using an analysis of variance to determine which parameters discriminated most between the size groups. Next, both classification algorithms were trained incrementally including additional parameters. Each instance of the models was cross-validated by dividing the training set in 8 subgroups, then the model was trained excluding one group. The sizes of this remaining groups of patients were fitted and compared to their true size. When performed for each subgroup this resulted in a mean accuracy score and a standard error.

Finally, the best scoring classifier of each type was applied to the patients with an AR grade ≥ 2. A chi-squared test was used to test whether the classification of the patients with an AR grade ≥ 2 was significantly different from the training set.

The analysis was performed in python 3.5 using the scikit-learn 0.17 machine learning module [Pedregosa et al., 2011].

Results

Of the 89 patients, 2 parameterizations failed and 2 did not receive an angiographic AR evaluation immediately after implantation. The remaining 85 patients were included in the analysis, 48 (57%) patients had an AR grade 0 or 1, 37 (43%) had an AR grade ≥ 2. Table 1 gives an overview of the distribution of the implant sizes in the population divided according to the severity of AR. The median aortic valve calcification volume was 195.8 mm^3, with the 25% quartile at 83.3 mm^3 and the 75% quartile at 335.7 mm^3.

Table 1: Implant sizes distribution in the patient population

CoreValve size [mm]	AR grade 0-1 (n = 48)	AR grade ≥ 2 (n = 37)
23		1
26	12 (25%)	9 (24%)
29	30 (62.5%)	18 (49%)
31	6 (12.5%)	9 (24%)

Statistical shape model

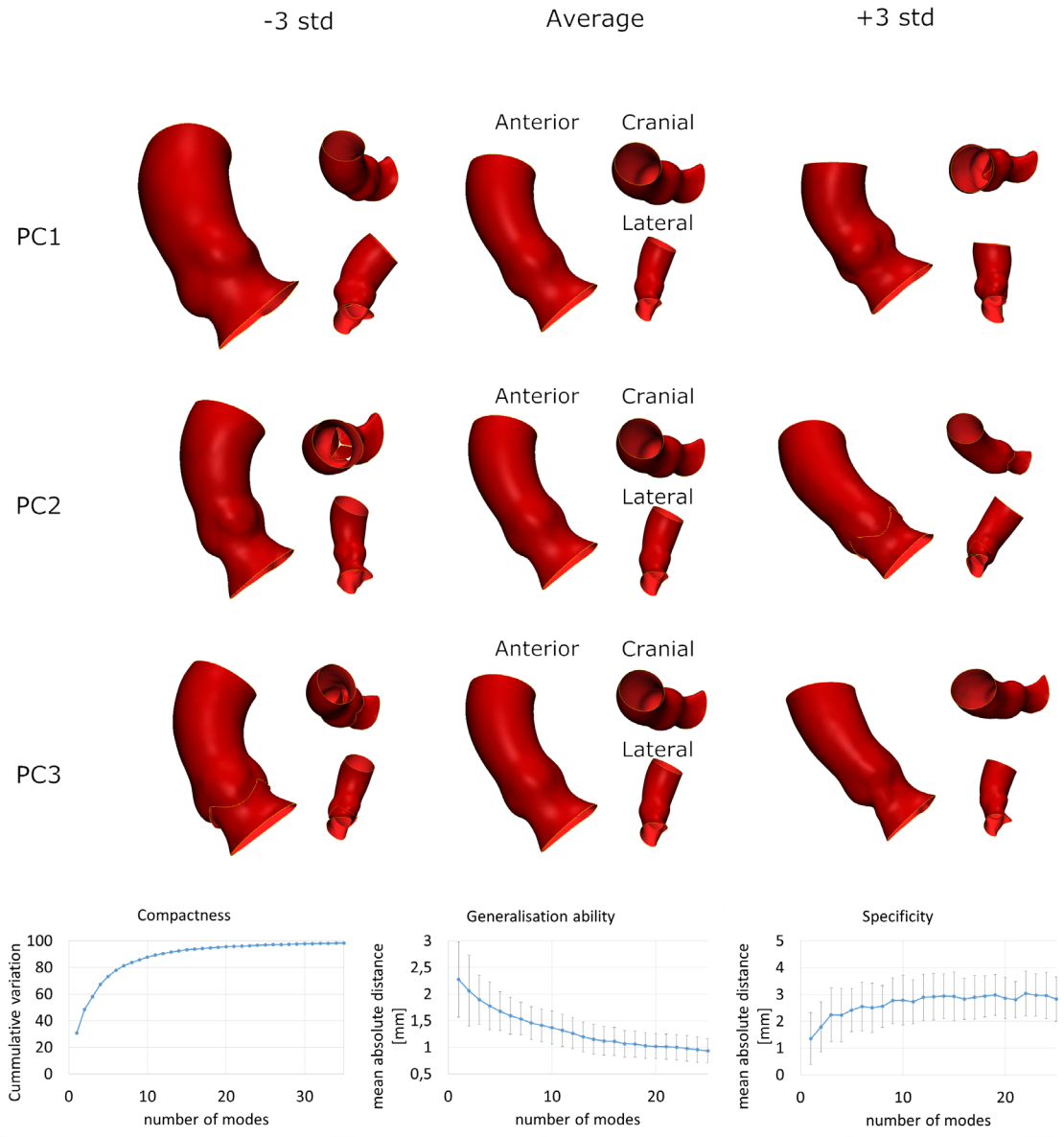

176

177 *Figure 3: A visualization of the first 3 principal components (PC) of the statistical shape model, the*
178 *anterior, cranial and lateral view of the average ± 3 standard deviations are shown. At the bottom,*
179 *the model characteristics are shown, from left to right, the compactness, generalization ability ± 1*
180 *standard deviation and specificity ± 1 standard deviation.*

181 Figure 3 depicts first 3 principal components and the compactness, generalization ability and
182 specificity of the SSM. The principal components have no intuitive, single physical interpretation such
183 as volume, size or angular deformation for example. The compactness analysis shows that 48% of all
184 shape variation is combined in the first two principal components, 87% of the variation is in the first

10 principal components and 95% of the variation is in the 20 first principal components. The generalization ability shows that using the first 20 principal components, a new shape can be approximated with a mean absolute distance of 1 mm. Finally, randomly generated shapes are at a mean absolute distance of approximately 3 mm from the closest shape in the training population.

Sizing algorithm

Figure 4 depicts the result of the parameter selection analysis, both classification algorithms perform best using the 20% most discriminating features. These features are principal component 1, 10, 7 and 2 respectively. Figure 5 depicts principal components 7 and 10, principal components 1 and 2 are shown in figure 3.

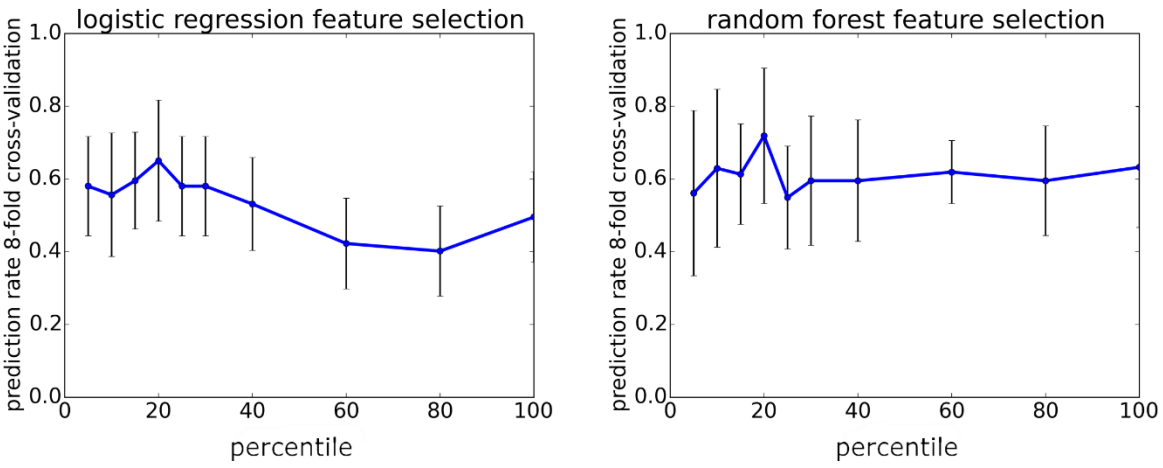

Figure 4: the result of the 8-fold cross-valdition and standard error for both classification algorithms as a function of the percentile of parameters included in the model

The linear model assigns 69% of the included patients the same size as they had implanted, the random forest classifier assigns the same size to 96% of the patients included in the model. Table 2 gives an overview of the cross-validation results for both models. It shows that both models do not assign a 31 mm implant to any of the patients in the cross-validation.

Table 2: Cross-validation of the training set, showing the number of correctly assigned sizes

CoreValve size [mm]	Linear model (60%)	Random forest classifier (65%)

26 (n = 12)	4 (33%)	7 (58.3%)
29 (n = 30)	25 (83%)	24 (80%)
31 (n = 6)	0	0

202

203 Table 3 contains the results of both classification algorithms on the patients with AR ≥ 2. The average
204 difference between the predicted size and the implanted size is -0.14 ± 2.04 mm for the random
205 forest classifier and -0.19 ± 1.90 mm for the linear model classifier. The random forest classifier
206 assigned the same size to 16 out of 36 patients with AR ≥ 2, 10 patients got one size larger, 1 got two
207 sizes larger and 9 got one size smaller. The generalized linear model assigned the same size to 18
208 patients, one size larger to 12 patients and one size smaller to 6 patients. In 72% of the patients both
209 models assigned the same size. However, the classification of the patients with AR ≥ 2 is not
210 significantly different from the cross-validation of the training set (random forest classifier: p = 0.28).
211 Also, specifically for the 29 mm size subgroups there is no statistical significant difference (random
212 forest classifier: p = 0.33).

213 *Table 3: Implant sizes assigned to patients with AR ≥ 2*

CoreValve size [mm]	**Linear model (46%)**	**Random forest classifier (43%)**
26 (n = 9)	2 (22%)	3 (33%)
29 (n = 18)	14 (78%)	11 (61%)
31 (n = 9)	1 (11%)	2 (22%)

214

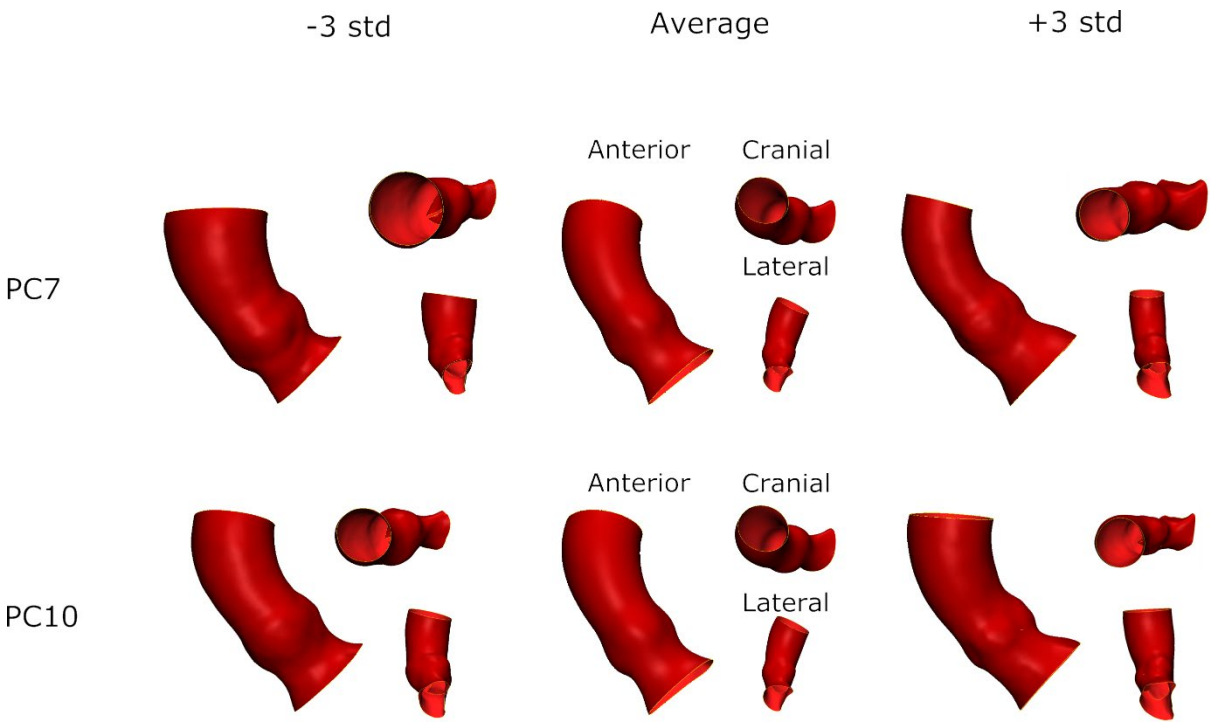

Figure 5: A visualization of principal components (PC) 7 and 10 of the statistical shape model, the anterior, cranial and lateral view of the average ± 3 standard deviations are show.

Discussion

The Goal of this research was to construct a method to base the sizing of the aortic root for implant selection on its 3D shape. The method described in this research used the weights associated with the principal components of a SSM as a parametric description of the 3D shapes in the population. The weights and the volume of calcification of the aortic valve were used as parameters in two classification algorithms: a generalized linear model and a random forest classifier. The classification algorithms were trained using the patients who did not suffer from AR or only suffered from mild AR (grade 1) after implantation of the device, assuming that those patients received the optimal implant size. Especially, the random forest classifier performed well, assigning the correct size to 96% of the patients included in the training set. Cross-validation showed that the subgroup of patients with a 31 mm implant did not contain enough patients to robustly train the algorithm when some were left out. Applying the trained algorithms to the patients with moderate to severe AR showed a lower

amount of patients being assigned the same size as was implanted, however the difference was not statistically significant.

Since the ideal implant size for each patient was in fact unknown it was impossible to determine whether the assigned sizes would improve the amount of regurgitation after the implantation. A potential method to compare the amount of AR with the implanted size versus the assigned size would be to simulate the implantation of both and virtually evaluate the amount of AR that would occur as described by [de Jaegere et al., 2016; Schultz et al., 2016].

The inclusion of the leaflets caused some artifacts in the SSM, as can be seen in principal component 3 in figure 3 where the leaflets protrude through the aortic wall in the -3 standard deviation extreme. This is most likely due to the separate registration and parameterization of both leaflets and the aortic root. Therefore, there is no physical connection in the model, nor correspondence, between the leaflet border and the aortic root. This can only be solved by constructing the correspondences of the leaflets and the wall as a whole.

The principal components describing the shape variation that were used in the classification algorithms had no straightforward physical interpretation. The first principal component contains a general size variation as can be seen in figure 3 and principal component 7 shows a local variation of the size of the left ventricular outflow. A potential method to make the model more intuitive is to associate interpretable morphological measures with the principal components through correlation as described by [Lacko et al., 2015].

In order to determine the size of a new patient's valve, the shape model needs to be fitted on the aortic root of that patient. The fit results in the weights associated with the principal components describing the new patient, these weights are then used in the classification algorithm. Two approaches can be devised to perform the fitting, either based on the displacement of corresponding points, therefore, the surface model of the aortic root needs to be corresponded with the SSM, or based on a fit of the surface using a non-rigid registration algorithm.

In conclusion, the proposed method was capable of accurately and semi-automatically assigning an implant size, using a CT scan of the aortic root. Additional data of patients in the less prevalent implant sizes is needed to make the algorithm more robust. In addition, the alternative sizes assigned to patients with moderate to severe AR need to be assessed to determine whether the occurrence of regurgitation diminishes.

Acknowledgements

This work was supported in part by a PhD grant from the *agency for innovation through science and technology (IWT)* of the Flemish government.

Conflicts of interest statement

Prof. Dr. Johan Bosmans is part-time clinical proctor for Medtronic. Prof. Dr. ir. Jos Vander Sloten is a member of the Board of Directors of Materialise N.V. and a shareholder. Dr. ir. Peter Mortier is CTO and shareholder of FEops N.V. The remaining authors have no conflicts of interest to declare.

References

Besl, P., McKay, N., 1992. A Method for Registration of 3-D Shapes. IEEE Trans. Pattern Anal. Mach. Intell.

Bose, A.K., Aitchison, J.D., Dark, J.H., 2007. Aortic valve replacement in octogenarians. J. Cardiothorac. Surg. 2, 33–5.

Boykov, Y., Kolmogorov, V., 2004. An experimental comparison of min-cut/max-flow algorithms for energy minimization in vision. IEEE Trans. Pattern Anal. Mach. Intell. 26, 1124–37.

Buzzatti, N., Maisano, F., Latib, A., Cioni, M., Taramasso, M., Mussardo, M., Colombo, A., Alfieri, O., 2013. Computed tomography-based evaluation of aortic annulus, prosthesis size and impact on early residual aortic regurgitation after transcatheter aortic valve implantation. Eur. J. Cardiothorac. Surg. 43, 43–50; discussion 50–1.

Davies, R.H., Twining, C.J., Cootes, T.F., Waterton, J.C., Taylor, C.J., 2002. A minimum description length approach to statistical shape modeling. IEEE Trans. Med. Imaging 21, 525–537.

de Jaegere, P., De Santis, G., Rodriguez-olivares, R., Bosmans, J., Bruining, N., Dezutter, T., Rahhab, Z., El Faquir, N., Collas, V., Bosmans, B., Verhegghe, B., Ren, C., Geleinse, M., Schultz, C., van Mieghem, N., De Beule, M., Mortier, P., 2016. Patient-specific computer modeling to predict aortic regurgitation after Transcatheter Aortic Valve Replacement. JACC. Cardiovasc. Interv. 9, 508–512.

Détaint, D., Lepage, L., Himbert, D., Brochet, E., Messika-Zeitoun, D., Iung, B., Vahanian, A., 2009. Determinants of significant paravalvular regurgitation after transcatheter aortic valve: implantation impact of device and annulus discongruence. JACC. Cardiovasc. Interv. 2, 821–7.

Ferrarini, L., Palm, W.M., Olofsen, H., Van Der Landen, R., Van Buchem, M.A., Reiber, J.H.C., Admiraal-Behloul, F., 2008. Ventricular shape biomarkers for Alzheimer's disease in clinical MR images. Magn. Reson. Med. 59, 260–267.

291 Hayashida, K., Bouvier, E., Lefèvre, T., Hovasse, T., Morice, M.-C., Chevalier, B., Romano, M., Garot,
292 P., Mylotte, D., Farge, A., Donzeau-Gouge, P., Cormier, B., 2012. Impact of CT-guided valve
293 sizing on post-procedural aortic regurgitation in transcatheter aortic valve implantation.
294 EuroIntervention 8, 546–55.

295 Holmes, D.R., Mack, M.J., Kaul, S., Agnihotri, A., Alexander, K.P., Bailey, S.R., Calhoon, J.H., Carabello,
296 B.A., Desai, M.Y., Edwards, F.H., Francis, G.S., Gardner, T.J., Kappetein, A.P., Linderbaum, J.A.,
297 Mukherjee, C., Mukherjee, D., Otto, C.M., Ruiz, C.E., Sacco, R.L., Smith, D., Thomas, J.D., 2012.
298 2012 ACCF/AATS/SCAI/STS Expert Consensus Document on Transcatheter Aortic Valve
299 Replacement. J. Am. Coll. Cardiol. 59, 1200–1254.

300 Huysmans, T., Sijbers, J., Verdonk, B., 2010. Automatic construction of correspondences for tubular
301 surfaces. IEEE Trans. Pattern Anal. Mach. Intell. 32, 636–51.

302 Jilaihawi, H., Kashif, M., Fontana, G., Furugen, A., Shiota, T., Friede, G., Makhija, R., Doctor, N., Leon,
303 M.B., Makkar, R.R., 2012. Cross-sectional computed tomographic assessment improves
304 accuracy of aortic annular sizing for transcatheter aortic valve replacement and reduces the
305 incidence of paravalvular aortic regurgitation. J. Am. Coll. Cardiol. 59, 1275–1286.

306 Kodali, S.K., Williams, M.R., Smith, C.R., Svensson, L.G., Webb, J.G., Makkar, R.R., Fontana, G.P.,
307 Dewey, T.M., Thourani, V.H., Pichard, A.D., Fischbein, M., Szeto, W.Y., Lim, S., Greason, K.L.,
308 Teirstein, P.S., Malaisrie, S.C., Douglas, P.S., Hahn, R.T., Whisenant, B., Zajarias, A., Wang, D.,
309 Akin, J.J., Anderson, W.N., Leon, M.B., 2012. Two-year outcomes after transcatheter or surgical
310 aortic-valve replacement. N. Engl. J. Med. 366, 1686–95.

311 Lacko, D., Huysmans, T., Parizel, P.M., De Bruyne, G., Verwulgen, S., Van Hulle, M.M., Sijbers, J., 2015.
312 Evaluation of an anthropometric shape model of the human scalp. Appl. Ergon. 48, 70–85.

313 Magnenat-thalmann, N., Seo, H., Cordier, F., 2004. Automatic Modeling of Virtual Humans and Body
314 Clothing. J. Comput. Sci. Technol. 19, 575–584.

315 Paulsen, R.R., Larsen, R., Nielsen, C., Laugesen, S., Ersbøll, B., 2002. Building and testing a statistical
316 shape model of the human ear canal. Med. Image Comput. Comput. Interv. 2489, 373–380.

317 Pedregosa, F., Varoquaux, G., Gramfort, A., Michel, V., Thirion, B., Grisel, O., Blondel, M.,
318 Prettenhofer, P., Weiss, R., Dubourg, V., Vanderplas, J., Passos, A., Cournapeau, D., Brucher, M.,
319 Perrot, M., Duchesnay, É., 2011. Scikit-learn: Machine Learning in Python. J. Mach. Learn. Res.
320 12, 2825–2830.

321 Ren, Y., Wang, L., Gao, Y., Tang, Z., Chen, K.C., Li, J., Shen, S.G.F., Yan, J., Lee, P.K.M., Chow, B., Xia,
322 J.J., Shen, D., 2014. Estimating anatomically-correct reference model for craniomaxillofacial
323 deformity via sparse representation. Lect. Notes Comput. Sci. (including Subser. Lect. Notes
324 Artif. Intell. Lect. Notes Bioinformatics) 8674 LNCS, 73–80.

325 Schultz, C., Rodriguez-olivares, R., Bosmans, J., Lefèvre, T., De Santis, G., Bruining, N., Collas, V.,
326 Dezutter, T., Bosmans, B., Rahhab, Z., El Faquir, N., Watanabe, Y., Segers, P., Verhegghe, B.,
327 Chevalier, B., van Mieghem, N., De Beule, M., Mortier, P., de Jaegere, P., 2016. Patient-specific
328 image-based computer simulation for the prediction of valve morphology and calcium
329 displacement after TAVI with the Medtronic CoreValve and the Edwards SAPIEN valve.
330 EuroIntervention 11, 1044–1052.

331 Schultz, C.J., Moelker, A., Piazza, N., Tzikas, A., Otten, A., Nuis, R.J., Neefjes, L.A., Van Geuns, R.J., De
332 Feyter, P., Krestin, G., Serruys, P.W., De Jaegere, P.P.T., 2010. Three dimensional evaluation of
333 the aortic annulus using multislice computer tomography: Are manufacturer's guidelines for
334 sizing for percutaneous aortic valve replacement helpful? Eur. Heart J. 31, 849–856.

335 Sellers, R.D., Levy, M.J., Amplatz, K., Lillehei, C.W., 1964. Left retrograde cardioangiography in
336 acquired cardiac disease: Technique, indications and interpretations in 700 Cases. Am. J.
337 Cardiol. 14, 437–447.

338 Styner, M. a, Rajamani, K.T., Nolte, L.-P., Zsemlye, G., Székely, G., Taylor, C.J., Davies, R.H., 2003.

339 Evaluation of 3D Correspondence Methods for Model Building. Proc. Inf. Process. Med. Imaging
340 18, 63–75.

341 Thourani, V.H., Ailawadi, G., Szeto, W.Y., Dewey, T.M., Guyton, R. a, Mack, M.J., Kron, I.L., Kilgo, P.,
342 Bavaria, J.E., 2011. Outcomes of surgical aortic valve replacement in high-risk patients: a
343 multiinstitutional study. Ann. Thorac. Surg. 91, 49–55; discussion 55–6.

344 Wang, Y., Yuan, L., Shi, J., Greve, A., Ye, J., Toga, A.W., Reiss, A.L., Thompson, P.M., 2013. Applying
345 tensor-based morphometry to parametric surfaces can improve MRI-based disease diagnosis.
346 Neuroimage 74, 209–230.

347 Zachow, S., Lamecker, H., Elsholtz, B., Stiller, M., 2005. Reconstruction of mandibular dysplasia using
348 a statistical 3D shape model. Int. Congr. Ser. 1281, 1238–1243.

Tables:

Figures: